Lecture 30

Fractal-like sets occurring in nature

This could be the subject of a book or, indeed, volumes of books. The discussion below will be brief – in no way does it pretend to be complete.

Benoit Mandelbrot's classic – and quite encyclopedic – work, *The Fractal Geometry of Nature* (W.H. Freeman, 1982) was concerned, as its name suggests, on the idea that fractal patterns occur in nature – not just here and there, but everywhere, e.g., clouds, rock, soil, river/tributary patterns, circulatory systems, etc.. His book was responsible for major shifts in research in most, if not all, areas of natural science.

Wherever there is branching, there is the possibility of "fractal-like" patterns. Of course, the word "branching" itself is closely connected with trees:

Left: Valley Oak tree. **Right:** Dawn Redwood tree.

Branching is also characteristic of river networks or "watersheds":

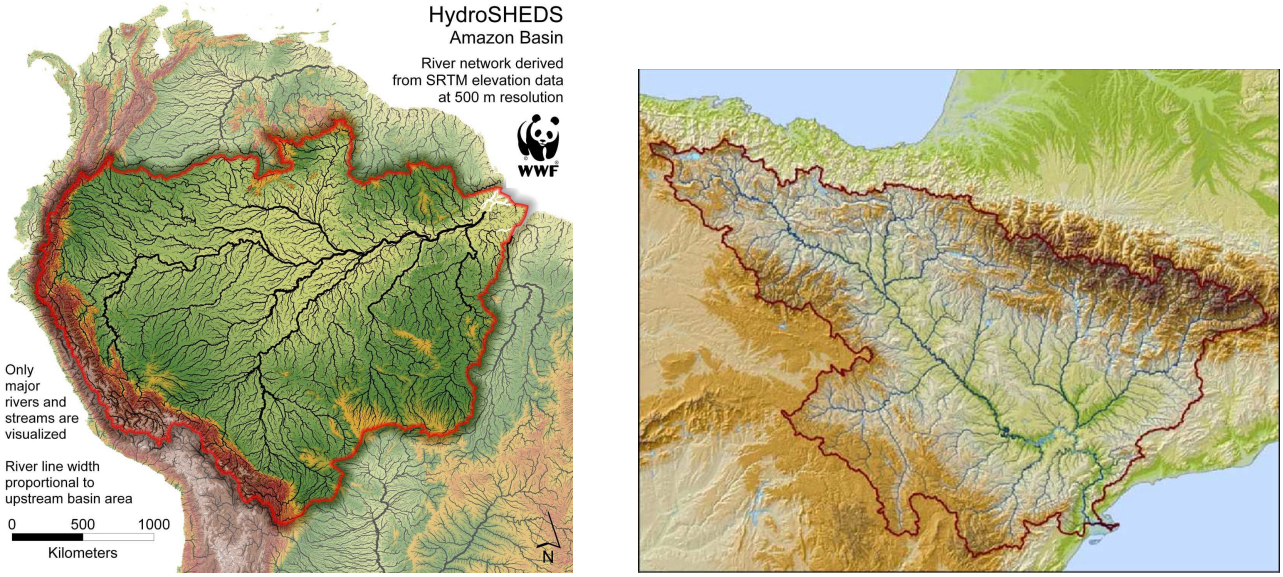

River networks. **Left:** Amazon river basin (Brazil). **Right:** Ebro river basin (Spain).

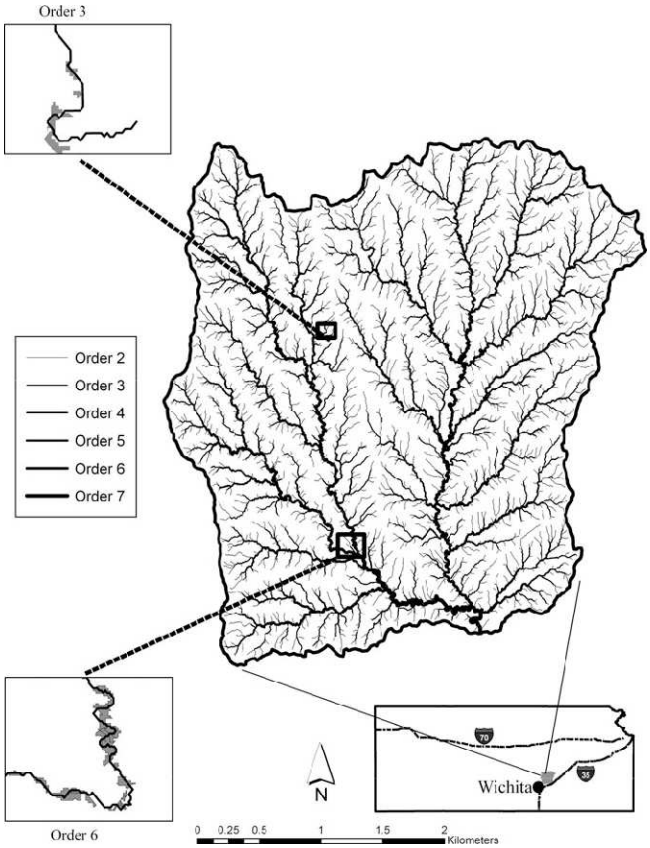

Whitewater River Network, Kansas, USA.

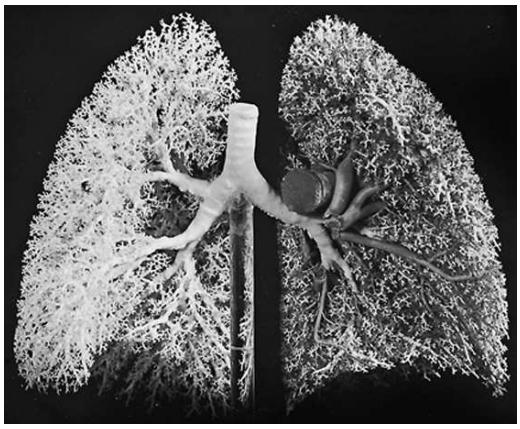

Human respiratory system: Bronchial tube network.

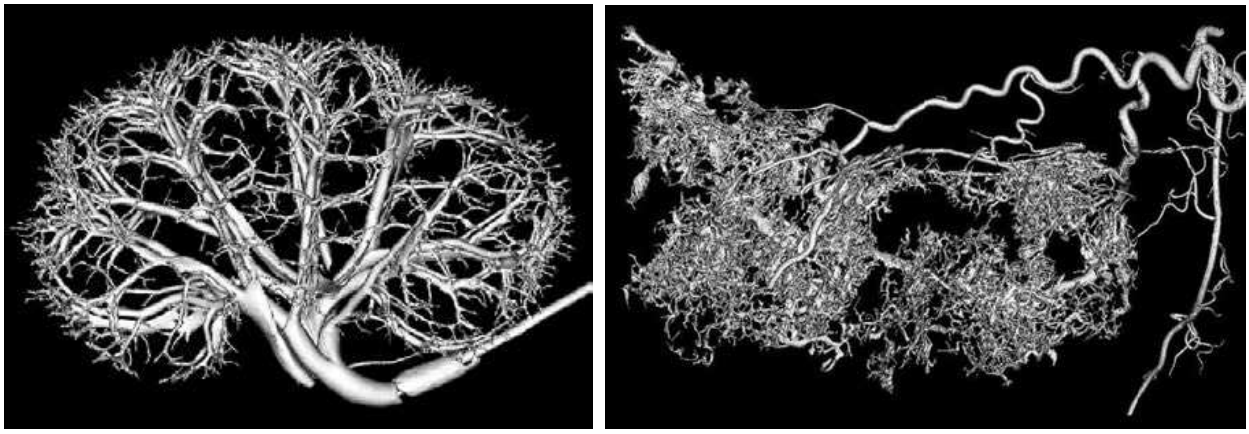

Renal (kidney) vasculature. **Left:** Healthy. **Right:** Tumorous.

Dendritic copper crystals.

Irregular surfaces and shapes in nature:

Lichens growing on tree bark.

Natural landscapes.

Artifically produced (computer generated) fractal landscapes.

Diffusion-limited aggregates as examples of fractal-like sets occurring in nature

An excerpt from the article entitled, "Diffusion-Limited Aggregation: A Model for Pattern Formation," by Thomas C. Halsey from the *Physics Today* online archive at the following site:

http://web.archive.org/web/20070405094836/http://aip.org/pt/vol-53/iss-11/p36.html

The basic concept

To understand the basics, consider colloidal particles undergoing Brownian motion in some fluid, and let them adhere irreversibly on contact with one another. Suppose further that the density of the colloidal particles is quite low, so one might imagine that the aggregation process occurs one particle at a time. We are then led to the following model.

Fix a seed particle at the origin of some coordinate system. Now introduce another particle at a large distance from the seed, and let it perform a random walk. Ultimately, that second particle will either escape to infinity or contact the seed, to which it will stick irreversibly. Now introduce a third particle into the system and allow it to walk randomly until it either sticks to the two-particle cluster or escapes to infinity. Clearly, this process can be repeated to an extent limited only by the modeler's patience and ingenuity (the required computational resources grow rapidly with n, the number of particles).

The clusters generated by this process are both highly branched and fractal. The cluster's fractal structure arises because the faster growing parts of the cluster shield the other parts, which therefore become less accessible to incoming particles. An arriving random walker is far more likely to attach to one of the tips of the cluster shown in the left figure (a) below than to penetrate deeply into one of the cluster's "fjords" without first contacting any surface site. Thus the tips tend to screen the fjords, a process that evidently operates on all length scales. Figure (b) at the right shows the "equipotential lines" of walker probability density near the cluster, confirming the unlikelihood of random walkers penetrating the fjords.

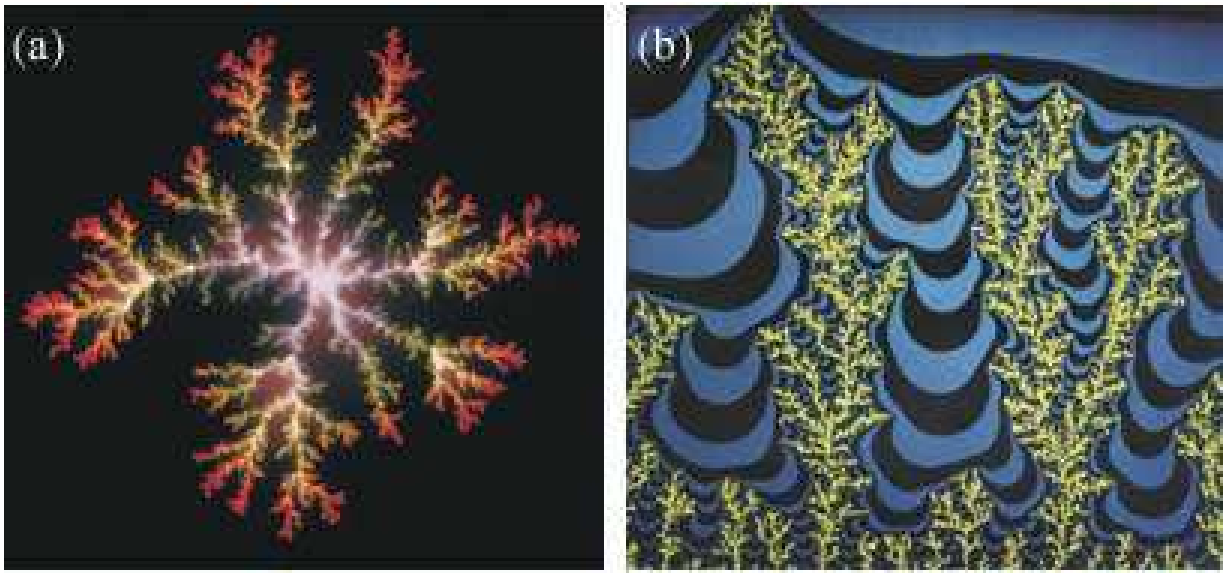

A theoretical cluster obtained by a computer simulation of this aggregation process is shown below.

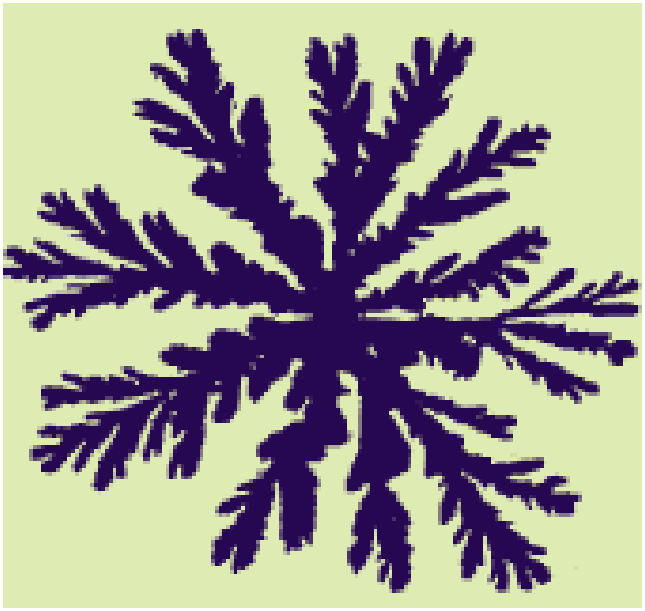

The fractal dimension D of both the theoretical as well as the experimental cluster in three-dimensions is roughly $D = 2.5$.

Generating tree-like sets

Because of the proliferation of tree-like objects in nature, one would naturally be motivated to devise methods of constructing them mathematically, perhaps by means of appropriate generators. The generators that were discussed earlier produce totally self-similar sets: Each component of the generator G is responsible for producing a contracted copy of the limiting fractal set S. (Recall that the classical von Koch curve may be considered as a union of four contracted copies of itself. Each copy was produced by one of the four components of the generator G.)

Trees or tree-like structures, which exhibit branching are, however, not perfectly self-similar. For example, consider the "fractal tree" shown below (we'll discuss how to generate it shortly):

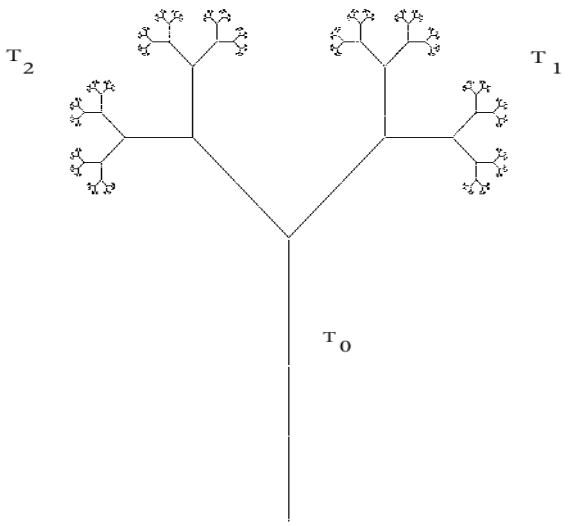

We can, of course, see copies of the entire tree – which we'll call "T" – within the tree: The two branches emanating from the trunk are the trunks of two "subtrees," denoted as T_1 and T_2, each of which is a contracted copy of the entire tree T. But there is also the trunk of the tree T, is denoted as T_0. The set T is therefore a union of the three sets T_i, $1 \leq i \leq 3$, i.e.,

$$T = T_0 \cup T_1 \cup T_2 \,. \tag{1}$$

Is the tree-like set T self-similar? In other words, can T be expressed as a union of copies of itself? It depends on whether or not we consider the set T_0, i.e., the one-dimensional trunk of T, as a contracted copy of T. And what is the answer? Well, there is no clear-cut answer. It depends on what you consider to be a "contracted" copy of a set. And there doesn't seem to be a standard answer in the research literature.

Some researchers (including the instructor of this course) consider the trunk T_0 as a "degenerate" copy of the set T – a "squashed down" version of T. It could be considered as the limit of a set of

contracted copies $T_{0,n}$ of T which become "flatter" as $n \to \infty$. But the problem is that we don't see anything of T in this set T_0. It could have been produced by "squashing" an infinite number of other sets.

One possible solution to this enigma is to state that the set T is not **strictly self-similar**. For a set S to be **strictly self-similar**, it would have to be expressible as a union of N contracted copies of itself, i.e., S_n, $1 \leq i \leq N$, with each copy S_n being produced by a contractive operation (i.e., a mapping) that is **invertible**. In other words, from each S_n, we can reconstruct the set S. (If we're dealing with linear contraction mappings, then a condition for invertibility would be that the linear mapping has nonzero determinant.) Using the above definition, we can then state that the tree T in the above figure is self-similar but not strictly self-similar.

In fact, it is because of its not-strictly-self-similar nature that we can identify a tree as a tree. If the tree were strictly self-similar, then every piece of the tree, i.e., every branch, would be a contracted version of the tree. If you think about it, we wouldn't have a tree with branches – we would have a self-similar set such as the Sierpinski triangle which clearly has no "branches." Recall also the fractal basin boundaries associated with Newton's method in the complex plane.

But this is getting far too complicated – beyond the scope of this course! Let's get "back to earth" and consider a simple family of generators which are designed to produce tree-like sets. Very simply, such generators must produce branching. Without loss of generality, we'll assume for the moment that the branching is **binary**, i.e., each branch of a tree will give rise to **two** sub-branches. (The number of sub-branches can be easily changed later.)

Shown below is a simple branching operation in the plane in which a branch, i.e., a line segment I of length l, will have two smaller sub-branches, of lengths $r_1 l$ and $r_2 l$, where $r_1, r_2 < 1$, added to one of its ends. Note that we must also specify the angles of orientation, θ_1 and θ_2, of the sub-branches, as shown in the figure.

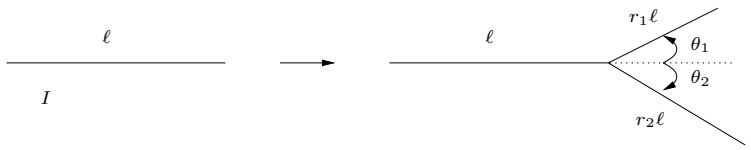

Simple branching generator G.

We may now continue this operation, with the understanding that at each iteration, **the generator G is applied only to the branches created in the previous iteration**. Another application of G to the set shown above produces the set shown below.
The set shown above can be considered to be the result of **two** applications of G to the original line segment of length ℓ.

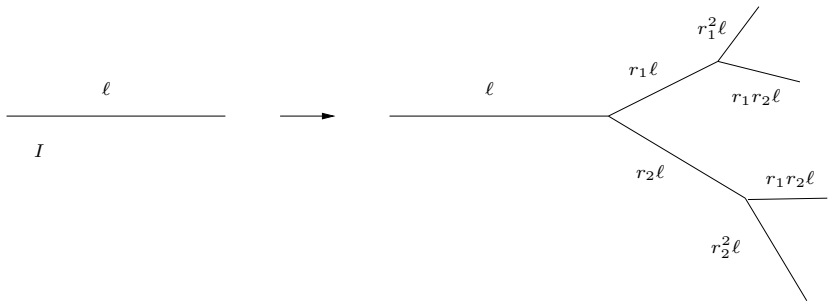

Simple branching generator G.

Subject to some conditions on the scaling factors r_1 and r_2 as well as the angles θ_1 and θ_2, repeated action of the generator G produces a set of finite trees $G^n(I)$ which, in the limit, $n \to \infty$, converge to a tree-like set T with finite size, as shown in the figure below. (Note that the relative magnitudes r_1 and r_2 are different from those of the generator shown above.)

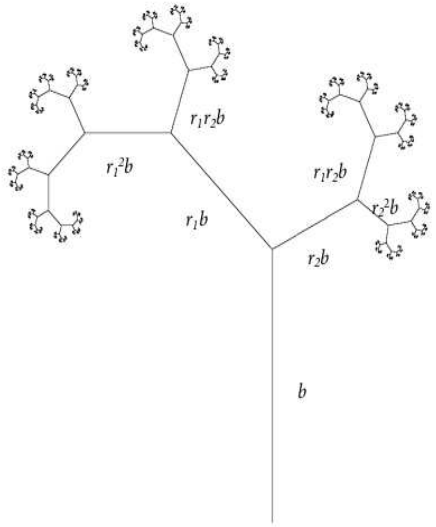

Limit tree-like set $T = \lim_{n\to\infty} G^n(I)$.

The tree T in the first figure of this section was produced with using a generator G with the following parameters,

$$r_1 = r_2 = \frac{1}{2}\,, \qquad \theta_1 = \theta_2 = \frac{\pi}{4}\,. \tag{2}$$

The determination of the fractal dimensions D of these tree-like sets is a little more complicated – not extremely difficult, but just a little more complicated – than the case of strictly self-similar sets such as the von Koch curves, Cantor-like sets and Sierpinski triangles examined earlier. Because of time constraints in this course, we shall have to omit a more detailed discussion of tree-like sets.

Estimating the (global) fractal dimension D of sets/objects

Given a set $S \in \mathbb{R}^k$, let $N(\epsilon)$ be the minimum number of k-dimensional balls of diameter ϵ in $\mathbb{R}^k$ needed to "cover" S, i.e., S is contained in a union of these balls. Recall that if S has fractal dimension D, then

$$N(\epsilon) \cong A\epsilon^{-D} = A\left(\frac{1}{\epsilon}\right)^D \quad \text{as} \quad \epsilon \to 0^+ . \tag{3}$$

If there are any doubts about this equation, let's verify it by showing that it produces a scaling result with which we are quite familiar. Assuming that (3) is correct, we have that the number of balls of diameter $r\epsilon$, where $0 < r < 1$, needed to cover S is

$$\begin{aligned} N(r\epsilon) &\cong A(r\epsilon)^{-D} \\ &= A\epsilon^{-D}r^{-D} \\ &= N(\epsilon)r^{-D} , \end{aligned} \tag{4}$$

which is our familiar scaling result.

For mathematical objects, the approximation in Eq. (3) improves as $\epsilon \to 0^+$. Now take logarithms of both sides of the above equation (it doesn't matter what base you choose for the logarithm),

$$\log N(\epsilon) \cong D \log\left(\frac{1}{\epsilon}\right) + \log A . \tag{5}$$

Rearranging,

$$D \cong \frac{\log N(\epsilon)}{\log \frac{1}{\epsilon}} - \frac{\log A}{\log \frac{1}{\epsilon}} . \tag{6}$$

As $\epsilon \to 0^+$, $\frac{1}{\epsilon} \to \infty$ which implies that $\log \frac{1}{\epsilon} \to \infty$ which, finally, implies that the second term in the above equation goes to zero. The mathematical definition of D is therefore

$$D = \lim_{\epsilon \to 0^+} \frac{\log N(\epsilon)}{\log \frac{1}{\epsilon}} , \tag{7}$$

provided that the limit exists. For all of the self-similar sets examined earlier, e.g., von Koch curves, Cantor-like sets, Sierpinski triangle, the above formula will yield the dimensions D that we obtained when we employ appropriate sequences of sizes/diameters ϵ_n which go to zero as $n \to 0$. We illustrate by returning to a couple of fractal sets studied early in this section.

Example No. 1: The von Koch curve. Recall that if we let $\epsilon_n = \frac{1}{3^n}$, $n \geq 1$, be the lengths of our measuring sticks, we need $N(\epsilon_n) = 4^n$ of these sticks to get from one end of the curve to the other. We also need $N(\epsilon_n) = 4^n$ square tiles with sides of length $\epsilon_n = \frac{1}{3^n}$ to cover the von Koch curve. Using the above formula, noting that $\epsilon_n \to 0$ as $n \to \infty$,

$$D = \lim_{n \to \infty} \frac{\log N(\epsilon_n)}{\log \frac{1}{\epsilon_n}} = \lim_{n \to \infty} \frac{\log 4^n}{\log 3^n} == \lim_{n \to \infty} \frac{n \log 4}{n \log 3} = \frac{\log 4}{\log 3} . \tag{8}$$

Lecture 31

Fractal-like sets occurring in nature (cont'd)

We return to the discussion near the end of the previous lecture.

Estimating the (global) fractal dimension D of sets/objects

Given a set $S \in \mathbb{R}^k$, let $N(\epsilon)$ be the minimum number of k-dimensional balls of diameter ϵ in $\mathbb{R}^k$ needed to "cover" S, i.e., S is contained in a union of these balls. Recall that if S has fractal dimension D, then

$$N(\epsilon) \cong A\epsilon^{-D} = A\left(\frac{1}{\epsilon}\right)^D \quad \text{as} \quad \epsilon \to 0^+ \,. \tag{9}$$

If there are any doubts about this equation, let's verify it by showing that it produces a scaling result with which we are quite familiar. Assuming that (9) is correct, we have that the number of balls of diameter $r\epsilon$, where $0 < r < 1$, needed to cover S is

$$\begin{aligned} N(r\epsilon) &\cong A(r\epsilon)^{-D} \\ &= A\epsilon^{-D}r^{-D} \\ &= N(\epsilon)r^{-D} \,, \end{aligned} \tag{10}$$

which is our familiar scaling result.

For mathematical objects, the approximation in Eq. (9) improves as $\epsilon \to 0^+$. Now take logarithms of both sides of the above equation (it doesn't matter what base you choose for the logarithm),

$$\log N(\epsilon) \cong D \log\left(\frac{1}{\epsilon}\right) + \log A \,. \tag{11}$$

Rearranging,

$$D \cong \frac{\log N(\epsilon)}{\log \frac{1}{\epsilon}} - \frac{\log A}{\log \frac{1}{\epsilon}} \,. \tag{12}$$

As $\epsilon \to 0^+$, $\frac{1}{\epsilon} \to \infty$ which implies that $\log \frac{1}{\epsilon} \to \infty$ which, finally, implies that the second term in the above equation goes to zero. The mathematical definition of D is therefore

$$D = \lim_{\epsilon \to 0^+} \frac{\log N(\epsilon)}{\log \frac{1}{\epsilon}} \,, \tag{13}$$

provided that the limit exists. For all of the self-similar sets examined earlier, e.g., von Koch curves, Cantor-like sets, Sierpinski triangle, the above formula will yield the dimensions D that we obtained when we employ appropriate sequences of sizes/diameters ϵ_n which go to zero as $n \to 0$. We illustrate by returning to a couple of fractal sets studied early in this section.

Example No. 1: The von Koch curve. Recall that if we let $\epsilon_n = \frac{1}{3^n}$, $n \geq 1$, be the lengths of our measuring sticks, we need $N(\epsilon_n) = 4^n$ of these sticks to get from one end of the curve to the other. We also need $N(\epsilon_n) = 4^n$ square tiles with sides of length $\epsilon_n = \frac{1}{3^n}$ to cover the von Koch curve. Using the above formula, noting that $\epsilon_n \to 0$ as $n \to \infty$,

$$D = \lim_{n\to\infty} \frac{\log N(\epsilon_n)}{\log \frac{1}{\epsilon_n}} = \lim_{n\to\infty} \frac{\log 4^n}{\log 3^n} == \lim_{n\to\infty} \frac{n \log 4}{n \log 3} = \frac{\log 4}{\log 3}\,. \tag{14}$$

Example No. 2: The ternary Cantor set. If we once again let $\epsilon_n = \frac{1}{3^n}$, $n \geq 1$, be the lengths of our measuring sticks, we need $N(\epsilon_n) = 2^n$ of these sticks to get from one end of the Cantor set to the other. Using the above formula, once again noting that $\epsilon_n \to 0$ as $n \to \infty$,

$$D = \lim_{n\to\infty} \frac{\log N(\epsilon_n)}{\log \frac{1}{\epsilon_n}} = \lim_{n\to\infty} \frac{\log 2^n}{\log 3^n} == \lim_{n\to\infty} \frac{n \log 2}{n \log 3} = \frac{\log 2}{\log 3}\,. \tag{15}$$

For natural objects, one will not be able to let $\epsilon \to 0^+$. As such, we shall have to determine $N(\epsilon)$ over a range of "reasonable" ϵ-values. We now outline the basic idea behind the estimation of fractal dimensions of "real" data sets.

Basic idea behind the estimation of the fractal dimension D of a data set

1. We work with a finite set of epsilon values, i.e., $\epsilon_1 > \epsilon_2 > \cdots \epsilon_n$, e.g.,

   $$\epsilon_k = r^k\,, \tag{16}$$

   where $0 < r < 1$ is a convenient scaling factor, possibly relevant to the problem.

   On a computer, this is often done with a digital image by using dyadic squares of pixels. For example, if our set S of concern is shown in a 512×512-pixel digital image, we let $\epsilon_1 = 512$, $\epsilon_2 = 512/2 = 256$, $\epsilon_3 = 256/2 = 128$, $\cdots$, $\epsilon_9 = 1$. Then $N(\epsilon_n)$ is the number of $\epsilon_n \times \epsilon_n$-pixel blocks needed to cover the set S. A single pixel represents the smallest ϵ-tile used to cover the set S. In this case, $N(\epsilon_9)$ will be the number of pixels needed to cover S. $N(\epsilon_8)$ will be the number of (nonoverlapping) 2×2-pixel blocks needed to cover S, and so on.

2. For $k = 1, 2, \cdots$, determine $N(\epsilon_k)$, the number of ϵ_k-balls (tiles) needed to cover S. (Since $N(\epsilon_1) = 1$, we don't expect it to be very useful in the computation.)

3. Plot $\log N(\epsilon_k)$ vs. $\log \dfrac{1}{\epsilon_k}$ for $1 \leq k \leq n$.

4. A least-squares fit to this data will produce a straight line with slope m that will be an approximation to D.

We illustrate this idea with a couple of examples below.

Experiment No. 1

Shown in the figure below is a 512×512-pixel digital image of a modified Sierpinski triangle. (It is obtained in the same way as before, i.e., by taking the middle-quarters. But here, we started with a right triangle as initial "seed.") Our fractal set S consists of all pixels which are black.

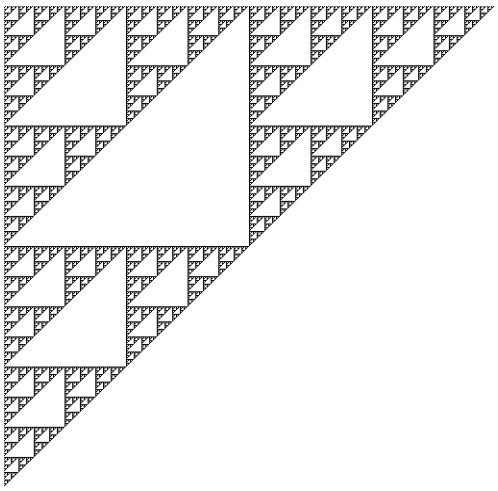

A simple computer program was written (in MATLAB) to perform "box counting" on this set using boxsizes of $\epsilon = 1, 2, 4, 8, 16$ and 32. (It is not very useful to use higher values of ϵ, since very few boxes are used.) The numbers of tiles $N(\epsilon)$ needed to cover the set S for these ϵ-values are shown in the table below.

ϵ	$N(\epsilon)$
32	81
16	243
8	729
4	2187
2	6561
1	19683

A plot of the values of $N(\epsilon)$ vs. $\log(1/\epsilon)$ from the above table is shown below.
The plot seems to indicate that the points lie very close to a straight line. Indeed, a least-squares fitting of the data yields a slope of

$$D \approx 1.5860\,, \tag{17}$$

which agrees extremely well with the theoretical result discussed earlier,

$$D = \frac{\ln 3}{\ln 2} \approx 1.5860\,. \tag{18}$$

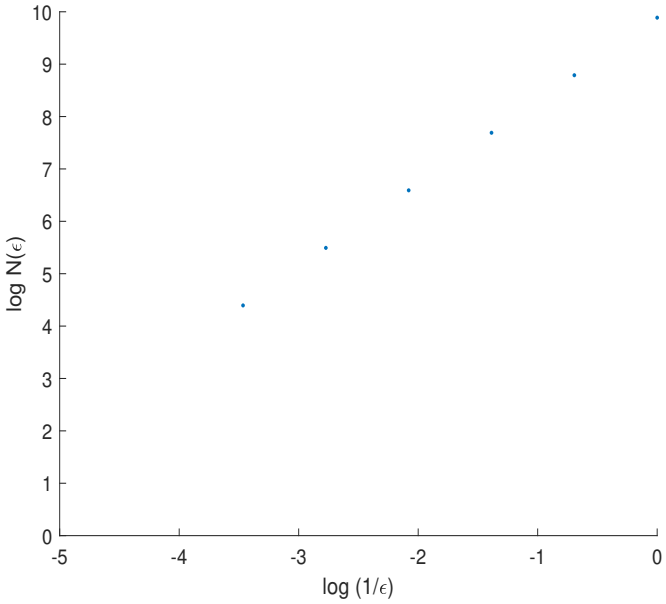
10
9
8
7
6
5
4
3
2
1
0
log N(ϵ)
-5
-4
-3
-2
-1
0
log (1/ϵ)

Experiment No. 2

The result of the above experiment may seem rather contrived since we used a "perfect" fractal, i.e., the Sierpinski gasket, even though it was a finite-dimensional representation of the gasket. Let us now consider a more realistic example, as presented in the figure below. It is a 512×512 digital image of the vasculature (blood vessels) in a tiny section of a a mouse ear obtained by a rather and novel method of imaging being developed at UW:

http://www.photomedicinelabs.com

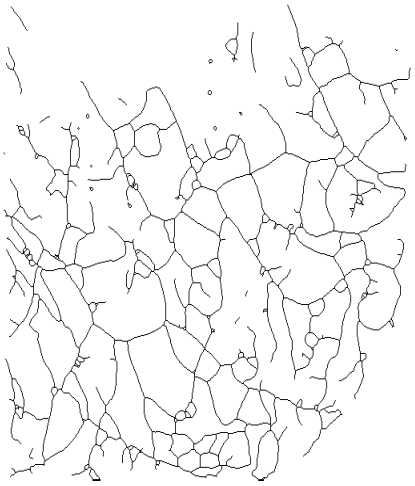

The computer program used in Experiment No. 1 was used once again to perform a box-counting analysis of the mouse ear image. As before, box sizes of $\epsilon = 1, 2, 4, 8, 16$ and 32 were used. The results are shown below.

ϵ	$N(\epsilon)$
32	218
16	631
8	1435
4	2970
2	5657
1	9568

A plot of the values of $N(\epsilon)$ vs. $\log(1/\epsilon)$ from the above table is shown below.

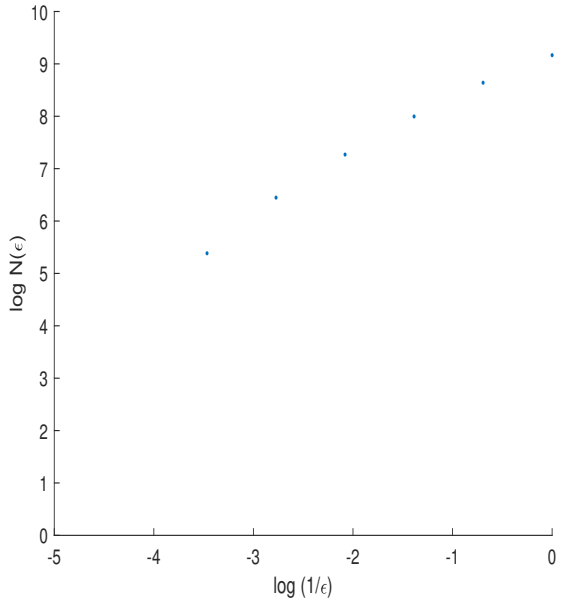

The points could be imagined to lie roughly on a straight line. If we fit a straight line using least-squares to all six points, the value of the slope is

$$D \cong 1.16\,, \tag{19}$$

which suggests that the network of blood vessels is slightly thicker than a simple curve. This estimate, however, might seem a little too low, given the complexity of the network.

If we look at the plot of $N(\epsilon)$ vs. $\log(1/\epsilon)$ values, we see that it flattens out as $\log(1/\epsilon)$ approaches 0, i.e., ϵ approaches 1. It may well be that using too fine a grid, i.e., boxes of lengths 2 and 1, is detecting only the curves. One can see this effect in the table of $N(\epsilon)$ values. As ϵ decreases from 4 to 2 to 1, the values of $N(\epsilon)$ are not increasing as rapidly as they were for higher values of ϵ.

For this reason, it may be desirable to use only the larger boxes, say, $\epsilon = 32, 16$ and 8. If we look at only the first three points (from the left) of the plot, they seem to lie close to a line with higher slope. Indeed, if we perform a least-squares fit on only these three points, we obtain a slope of

$$D \cong 1.35\,, \tag{20}$$

which is a significant increase from the previous value.

This motivates the use of even larger box sizes. If we use $\epsilon = 64$ and 128 sized boxes, we obtain the following additional counts:

ϵ	$N(\epsilon)$
128	16
64	60

A plot of the logarithms of these values, along with those of the three points used earlier, is shown below. A least-squares fit through these five points yields a line with slope,

$$D \cong 1.64\,. \tag{21}$$

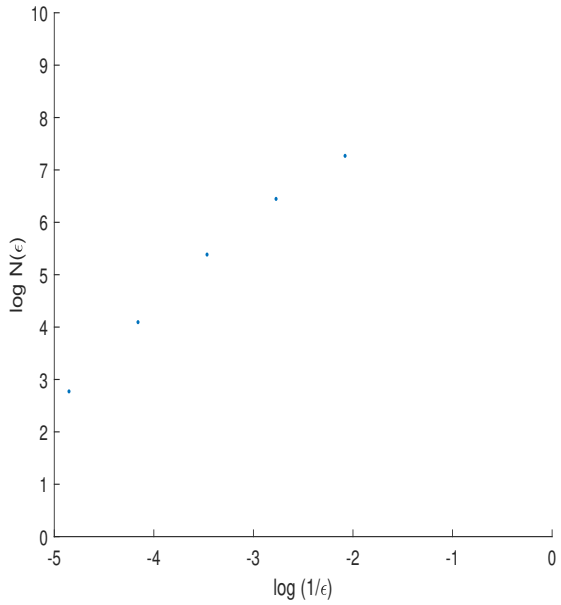

Our box-counting method seems to be detecting a set which is thicker than a curve but thinner than a planar area. That being said, the above analysis may seem somewhat unsettling to the reader since a definitive result is not obtained. Is the fractal dimension D of the vasculature closer to 1.2? Or is it closer to 1.6. It might seem that D is closer to 1.6 but we can't be too precise. One reason is that we don't have enough data to answer this question. But the other point that should be made is that the "fractal scaling" exhibited by the vasculature is dependent upon the scales that we use, i.e., the sizes of boxes used, in our covering. Unlike mathematical objects, we cannot go to infinitely small scales. We have to acknowledge that the scaling properties discussed earlier for mathematical fractals hold only over a finite range of scales for objects in the real world.

Iterated function systems (IFS) and the construction of fractal sets

We now discuss a very convenient and powerful method of constructing and analyzing self-similar fractal sets – the so-called method of **iterated function systems**, abbreviated as **IFS**. The IFS method will involve the use of a set **contractive mappings** on the line $\mathbb{R}$, or in the plane $\mathbb{R}^2$ or in 3D space $\mathbb{R}^3$. as opposed to the generators discussed in the previous lectures. In this way, one doesn't have to keep track of line segments and then operating on them. A remarkable aspect of the IFS method is that one can generate very good pictures of fractals by simply applying the maps in an IFS in a random manner, as was discussed in Problem Set No. 5.

We'll illustrate the idea with a simple example – the one, in fact, that was used in Problem Set No. 5. From that example, we'll move on to a more general discussion, and then look a little more closely at the mathematics behind IFS.

Consider the following two maps, f_1 and f_2, which map the interval $I = [0,1]$ into itself: For any $x \in [0,1]$, $f_1(x) \in [0,1]$ and $f_2(x) \in [0,1]$:

1. $f_1(x) = \frac{1}{3}x$ with fixed point $\bar{x}_1 = 0$. The iteration dynamics associated with $f_1(x)$ is quite straightforward: For any $x_0 \in [0,1]$, $x_n = f_1^n(x_0) = \frac{x_0}{3^n} \to 0$ as $n \to \infty$.

2. $f_2(x) = \frac{1}{3}x + \frac{2}{3}$ with fixed point $\bar{x}_2 = 1$. The iteration dynamics associated with $f_2(x)$ is also quite straightforward: The distance between $x_{n+1} = f_2(x_n)$ and the fixed point $\bar{x}_2 = 1$ is one-third the distance between the point x_n and $\bar{x}_2$. As such, $x_n = f_2^n(x_0) \to 1$ as $n \to \infty$.

We now examine the (repeated) action of the maps f_1 and f_2 **on the interval** $I = [0,1]$. Instead of looking at where each map f_i sends a point $x \in [0,1]$, we consider where each map f_i will send **sets of points in [0,1]**. It is instructive to examine the action of each of the above maps on the interval [0,1]. To do this, let us define the following associated **interval-** or **set-valued mappings**:

Definition: For $i \in \{1,2\}$ and any subset $S \subseteq [0,1]$, we denote $\hat{f}_i(S) = \{f_i(x) | x \in S\}$.

To illustrate:

1. $\hat{f}_1([0,1]) = [0, \frac{1}{3}]$. In other words, $\hat{f}_1$ "shrinks" the interval [0,1] to $[0, \frac{1}{3}]$.

2. $\hat{f}_2([0,1]) = [\frac{2}{3}, 1]$. In other words, $\hat{f}_2$ "shrinks" the interval $[0,1]$ to $[\frac{2}{3}, 1]$.

It might help to use some pictures. Let's consider map f_1 for the moment. If we let $I_0 = [0,1]$, then the interval $I_1 = \hat{f}_1(I_0) = [0, \frac{1}{3}]$ is sketched below. We then apply $\hat{f}_1$ to the set I_1 to produce the set $I_2 = \hat{f}_1(I_1) = [0, \frac{1}{9}]$.
In general, n applications of the map $\hat{f}_1$ to the interval I_0 produces the set

$$I_n = \hat{f}_1(I_0) = \left[0, \frac{1}{3^n}\right] . \tag{22}$$

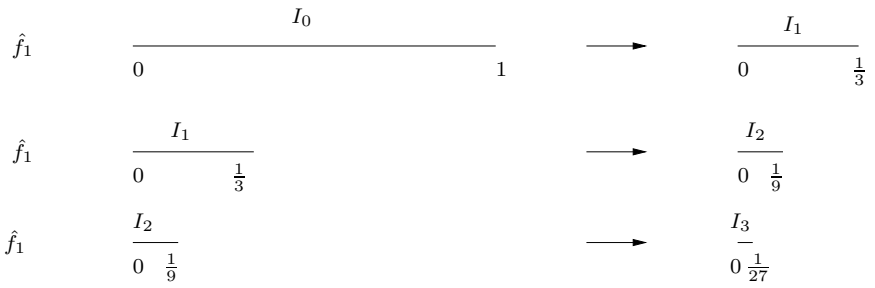

Clearly, the intervals I_n are shrinking in length. Moreover, they appear to be approaching a limit, i.e.,

$$\lim_{n\to\infty} I_n = \lim_{n\to\infty} \left[0, \frac{1}{3^n}\right] = \{0\}\,. \tag{23}$$

They are approaching the single point $\{0\}$. Note that this point is the fixed point of f_1. We may view this single point as a set or an interval consisting of one point.

Let's now consider the map f_2. If we let $I_0 = [0, 1]$, then the interval $I_1 = \hat{f}_2(I_0) = [\frac{2}{3}, 1]$ is sketched below. We then apply $\hat{f}_2$ to the set I_1 to produce the set $I_2 = \hat{f}_1(I_1) = [\frac{8}{9}, 1]$. This procedure is shown graphically below.

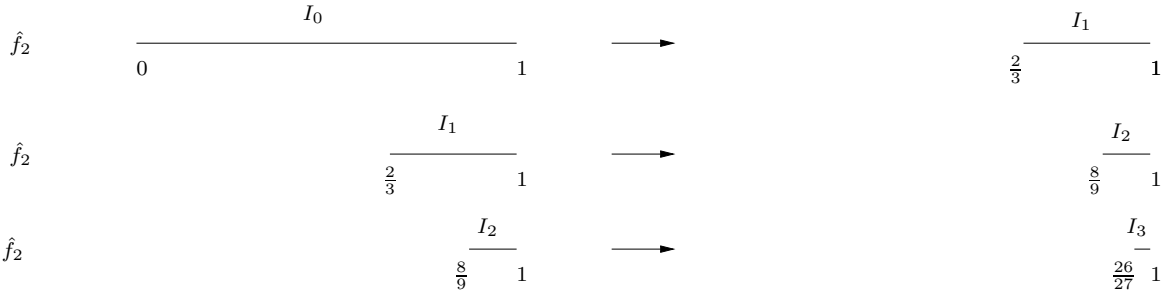

In general, n applications of the map $\hat{f}_2$ to the interval I_0 produces the set

$$I_n = \hat{f}_1(I_0) = \left[1 - \frac{1}{3^n}, 1\right] = \left[\frac{3^n - 1}{3^n}, 1\right]\,. \tag{24}$$

Once again, the intervals I_n are shrinking in length. Moreover, they appear to be approaching a limit, i.e.,

$$\lim_{n\to\infty} I_n = \lim_{n\to\infty} \left[1 - \frac{1}{3^n}, 1\right] = \{1\}\,. \tag{25}$$

They are approaching the single point $\{1\}$, which is the fixed point of f_2. We may once again view this single point as a set or an interval consisting of one point.

In summary:

1. Repeated application of the set-valued map $\hat{f}_1$ to the interval $I = [0, 1]$ produces a set of intervals I_n which are "shrinking" toward the fixed point $\bar{x}_1$ of f_1.

2. Repeated application of the set-valued map $\hat{f}_2$ to the interval $I = [0,1]$ produces a set of intervals I_n which are "shrinking" toward the fixed point $\bar{x}_2$ of f_2.

Now, instead of considering the action of each of the set-valued maps $\hat{f}_1$ and $\hat{f}_2$ separately, let's combine their actions as if they were components of a **"Parallel Machine".** We'll do this as follows:

For any subset $S \in [0,1]$, define that following set-valued mapping,

$$\hat{\mathbf{f}}(S) = \hat{f}_1(S) \cup \hat{f}_2(S)\,. \tag{26}$$

In other words, the set-valued mapping is the union of the actions of the individual maps $\hat{f}_1$ and $\hat{f}_2$. Let's examine the action of $\hat{\mathbf{f}}$ on the set $I_0 = [0,1]$:

$$\begin{aligned} I_1 = \hat{\mathbf{f}}([0,1]) &= \hat{f}_1([0,1]) \cup \hat{f}_2([0,1]) \\ &= \left[0, \frac{1}{3}\right] \cup \left[\frac{2}{3}, 1\right]. \end{aligned} \tag{27}$$

This is shown graphically below:

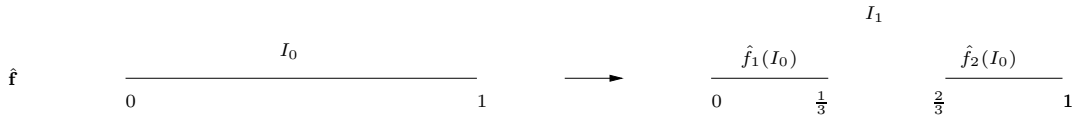

Now apply $\hat{\mathbf{f}}$ to the set I_1:

$$\begin{aligned} I_2 = \hat{\mathbf{f}}(I_1) &= \hat{f}_1(I_1) \cup \hat{f}_2([I_1) \\ &= \left(\left[0, \frac{1}{9}\right] \cup \left[\frac{2}{9}, \frac{1}{3}\right]\right) \cup \left(\left[\frac{2}{3}, \frac{7}{9}\right] \cup \left[\frac{8}{9}, 1\right]\right) \\ &= \left[0, \frac{1}{9}\right] \cup \left[\frac{2}{9}, \frac{1}{3}\right] \cup \left[\frac{2}{3}, \frac{7}{9}\right] \cup \left[\frac{8}{9}, 1\right]. \end{aligned} \tag{28}$$

This is shown graphically below:

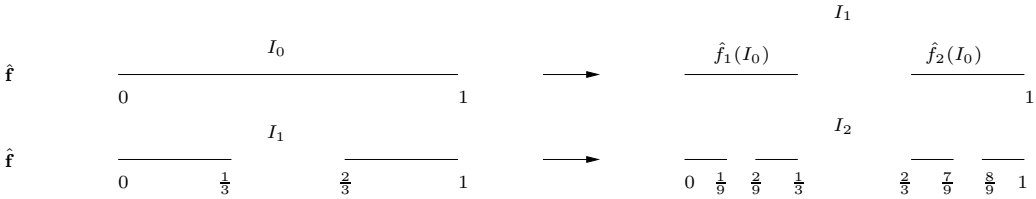

We see that **the repeated application of the "parallel machine" $\hat{\mathbf{f}}$ performs the "middle-thirds dissection procedure" that was employed in the construction of the ternary Cantor set C in $[0,1]$:**

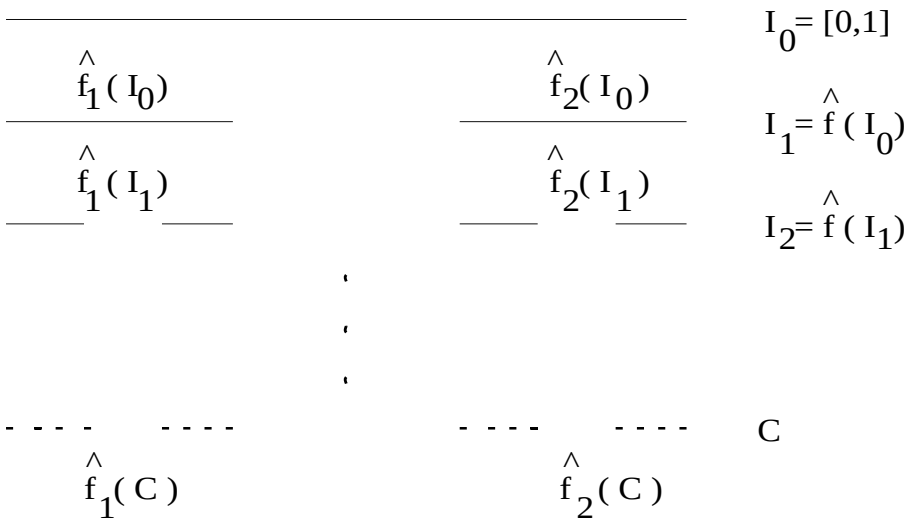

If we consider the following iteration process involving the parallel map $\hat{\mathbf{f}}$:

$$I_{n+1} = \hat{\mathbf{f}}(I_n) = \hat{f}_1(I_n) \cup \hat{f}_2(I_n)\,, \tag{29}$$

then it appears that

$$\lim_{n\to\infty} I_n = C\,, \quad \text{ternary Cantor set in [0,1]}\,. \tag{30}$$

But the story is not over! As shown in the figure above, **the ternary Cantor set C is a "fixed point" of the parallel operator $\hat{\mathbf{f}}$**, i.e.,

$$C = \hat{\mathbf{f}}(C) = \hat{f}_1(C) \cup \hat{f}_2(C)\,. \tag{31}$$

In other words, $\hat{\mathbf{f}}$ maps **the set** C to itself.

Recalling that the set-valued maps $\hat{f}_1$ and $\hat{f}_2$ "shrink" sets, we see that:

The ternary Cantor set C is a union of shrunken copies of itself.

We actually noticed this earlier, but we didn't really specify the maps that produced these copies. Now, we can identify the maps that produce the copies – the two maps $\hat{f}_1$ and $\hat{f}_2$ that comprise the "parallel operator" $\hat{\mathbf{f}}$.

Lecture 32

Iterated function systems (IFS) and the construction of fractal sets (cont'd)

We continue with our discussion from the previous section in order to discuss in more detail the mathematical aspects of IFS. Previously, we considered the parallel action of the two maps

$$f_1(x) = \frac{1}{3}x\,, \qquad f_2(x) = \frac{1}{3}x + \frac{2}{3}\,. \tag{32}$$

(Actually, we looked at the set-valued maps associated with these maps, but we'll skip that detail for now.) Repeated iteration of these maps produced the ternary Cantor set on $[0, 1]$.

The above system of two maps acting in parallel is a particular example of an **iterated function system** (IFS). For the moment, we shall provide a "working definition" of an IFS in $\mathbb{R}^n$. But we must first provide a couple of other useful definitions.

Distance function/metric in $\mathbb{R}^n$: Let $x, y \in \mathbb{R}^n$. We shall let $d(x, y)$ denote the (Euclidean) distance between x and y. In the special case $n = 1$,

$$d(x, y) = |x - y|\,, \quad x, y \in \mathbb{R}\,. \tag{33}$$

For $n \geq 1$, where $x = (x_1, x_2, \cdots, x_n)$ and $y = (y_1, y_2, \cdots, y_n)$,

$$d(x, y) = \|x - y\| = \left[\sum_{k=1}^{n}(x_k - y_k)^2\right]^{1/2}, \quad x, y \in \mathbb{R}^n\,. \tag{34}$$

Note: Other distance functions/metrics can be used. We'll use the Euclidean distance for simplicity.

Definition (Contraction Mapping): Let $D \subseteq \mathbb{R}^n$ and $f : D \to D$. We say that f is a **contraction mapping** on D if there exists a constant $0 \leq C < 1$ such that

$$d(f(x), f(y)) \leq C d(x, y) \quad \text{for all } \; x, y \in D\,. \tag{35}$$

The smallest C for which the above inequality holds is called the **contraction factor** of f. **Note that the contraction factor must be strictly less than 1.**

In other words, a contraction mapping f maps any two distinct points x and y closer to each other.

Examples: Most of our discussion of IFS will be limited to $\mathbb{R}$ and $\mathbb{R}^2$, so the following examples should be sufficient.

1. The maps f_1 and f_2 examined earlier are contraction mappings on $\mathbb{R}$. Consider $f_1(x) = \frac{1}{3}x$: For any $x, y \in \mathbb{R}$,

$$\begin{aligned} d(f_1(x), f_1(y)) &= |f_1(x) - f_1(y)| \\ &= \left|\frac{1}{3}x - \frac{1}{3}y\right| \\ &= \frac{1}{3}|x - y| \\ &= \frac{1}{3}d(x, y)\,. \end{aligned} \tag{36}$$

The distance between $f_1(x)$ and $f_2(y)$ is always one-third the distance between x and y. The contraction factor for $f_1(x) = \frac{1}{3}x$ is $C = \frac{1}{3}$.

Now consider $f_2(x) = \frac{1}{3}x + \frac{2}{3}$: For any $x, y \in \mathbb{R}$,

$$\begin{aligned} d(f_2(x), f_2(y)) &= |f_2(x) - f_2(y)| \\ &= \left|\left(\frac{1}{3}x + \frac{2}{3}\right) - \left(\frac{1}{3}y + \frac{2}{3}\right)\right| \\ &= \frac{1}{3}|x - y| \\ &= \frac{1}{3}d(x, y)\,. \end{aligned} \tag{37}$$

The contraction factor for $f_2(x) = \frac{1}{3}x + \frac{2}{3}$ is also $C = \frac{1}{3}$.

It will be useful to work with smaller subsets $D \subset \mathbb{R}$ over which these maps are contractions. With reference to the Cantor set example studied earlier, we can establish that each of the f_i maps the interval $[0, 1]$ to itself:

(a) For $x \in [0, 1]$, $f_1(x) = \frac{1}{3}x \in [0, 1]$. Therefore, f_1 maps [0,1] to itself.

(b) For $x \in [0, 1]$, $f_2(x) = \frac{1}{3}x + \frac{2}{3} \in [0, 1]$. Therefore, f_2 maps [0,1] to itself.

We could also use the set-valued versions of these maps to arrive at these results:

(a) $\hat{f}_1 : [0, 1] \to [0, \frac{1}{3}] \subset [0, 1]$. Therefore f_1 maps [0,1] to itself.

(b) $\hat{f}_1 : [0, 1] \to [\frac{2}{3}, 1] \subset [0, 1]$. Therefore f_2 maps [0,1] to itself.

Therefore f_1 and f_2 are contraction maps on the set $D = [0, 1]$.

In general, the following affine map on $\mathbb{R}$,

$$f(x) = ax + b\,, \tag{38}$$

is a contraction mapping on $\mathbb{R}$ if $|a| < 1$ in which case its contraction factor is $C = |a|$. For all $x, y \in \mathbb{R}$,

$$|f(x) - f(y)| = |a|\,|x - y|\,, \tag{39}$$

i.e., the distance between $f(x)$ and $f(y)$ is **exactly** $|a|$ times the distance between x and y. For nonlinear maps, such an equality will not exist and the best we can do is to find an inequality the distances. More on this later.

That being said, in most of the examples and applications examined for the remainder of this secction, affine maps will be employed.

2. Consider the following class of affine transformations in the plane $\mathbb{R}^2$,

$$f(\mathbf{x}) = \mathbf{A}\mathbf{x} + \mathbf{b}\,, \tag{40}$$

or, in coordinate form,

$$f(x_1, x_2) = \begin{pmatrix} a_{11} & a_{12} \\ a_{21} & a_{22} \end{pmatrix} \begin{pmatrix} x_1 \\ x_2 \end{pmatrix} + \begin{pmatrix} b_1 \\ b_2 \end{pmatrix}. \tag{41}$$

Note that for $\mathbf{x}, \mathbf{y} \in \mathbb{R}^2$,

$$f(\mathbf{x}) - f(\mathbf{y}) = \mathbf{A}(\mathbf{x} - \mathbf{y})\,. \tag{42}$$

This implies that

$$\begin{aligned} d(f(\mathbf{x}), f(\mathbf{y})) &= \|\mathbf{A}(\mathbf{x} - \mathbf{y})\|_2 \\ &\leq \|\mathbf{A}\|_2\, d(\mathbf{x}, \mathbf{y})\,, \end{aligned} \tag{43}$$

where $\|\mathbf{A}\|_2$ denotes the **(Euclidean) matrix norm** of $\mathbf{A}$, which you may have encountered in a course on linear algebra. It suffices to state here that a sufficient condition for the affine mapping f to be contractive is that $|\lambda_1| < 1$ and $|\lambda_2| < 1$, where the λ_i are the eigenvalues of $\mathbf{A}$.

Definition (iterated function system): Let $\mathbf{f} = \{f_1, f_2, \cdots, f_N\}$ denote a set of N contraction mappings on a closed and bounded subset $D \subset \mathbb{R}^n$, i.e., for each $k \in \{1, 2, \cdots N\}$, $f_k : D \to D$ and there exists a constant $0 \leq C_k < 1$ such that

$$d(f_k(x), f_k(y)) \leq C_k\, d(x, y) \quad \text{for all } x, y \in D\,. \tag{44}$$

Associated with this set of contraction mappings is the "parallel set-valued mapping" $\hat{\mathbf{f}}$, defined as follows: For any subset $S \subset D$,

$$\hat{\mathbf{f}}(S) = \bigcup_{k=1}^{n} \hat{f}_k(S)\,, \tag{45}$$

where the $\hat{f}_k$ denote the set-valued mappings associated with the mappings f_k. The set of maps $\mathbf{f}$ with parallel operator $\hat{\mathbf{f}}$ define an N-map **iterated function system (IFS)** on the set $D \subset \mathbb{R}^n$.

We now state the main result associated regarding N-map Iterated Function Systems as defined above.

Theorem: There exists a unique set $A \subset D$ which is the "fixed point" of the parallel IFS operator $\hat{\mathbf{f}}$, i.e.,

$$A = \hat{\mathbf{f}}(A) = \bigcup_{k=1}^{N} \hat{f}_k(A)\,. \tag{46}$$

Moreover, if you start with any set $S_0 \in D$ (even a single point $x_0 \in D$), and form the iteration sequence,

$$S_{n+1} = \hat{\mathbf{f}}(S_n)\,, \tag{47}$$

then the sequence of sets $\{S_n\}$ converges to the fixed-point set $A \subset D$. For this reason, A is known as the **attractor** of the IFS.

From Eq. (46) is that the set A is **self-similar**, i.e., A **is the union of** N **geometrically-contracted copies of itself**. We shall be examining this property in a number of examples below.

There are actually two practical consequences of the above result, depending upon one's perspective:

1. If you have a set of contraction maps $\mathbf{f} = \{f_k\}_{k=1}^{N}$, you can quickly construct "pictures" of the attractor set A. We'll discuss this in more detail a little later.

2. Given a self-similar, possibly fractal, set S, one may be able to determine the maps $\{f_k\}$ comprising the IFS $\mathbf{f}$ for which S is the attractor. This will then allow us to construct the "pictures" of S mentioned in 1. above without having to use "generators."

Examples of IFS and their (fractal) attractors

Cantor-like sets on [0,1]

At this point, it is instructive to look at some examples. We have already shown how the Cantor set C can be viewed as the attractor of a two-map IFS on [0,1], namely, the two maps,

$$f_1(x) = \frac{1}{3}x\,, \quad f_2(x) = \frac{1}{3}x + \frac{2}{3}\,. \tag{48}$$

Recall that both of these maps are contraction maps on $[0,1]$ with contractivity factors equal to $\frac{1}{3}$. This is due to the factor $\frac{1}{3}$ which multiplies x in each map. What would happen if we changed this factor? For example, consider the two maps,

$$f_1(x) = \frac{1}{4}x\,, \quad f_2(x) = \frac{1}{4}x + \frac{3}{4}\,. \tag{49}$$

Once again, we have $f_1(0) = 0$ and $f_2(1) = 1$. The action of the IFS parallel map $\hat{\mathbf{f}}$ composed of these two maps on the interval $I_0 = [0, 1]$ is as follows:

$$\begin{aligned} \hat{\mathbf{f}}([0,1]) &= \hat{f}_1([0,1]) \bigcup \hat{f}_2([0,1]) \\ &= \left[0, \frac{1}{4}\right] \bigcup \left[\frac{3}{4}, 1\right] \\ &= I_1 \,. \end{aligned} \tag{50}$$

The action of $\hat{\mathbf{f}}$ on an interval is to remove the middle one-half of the interval:

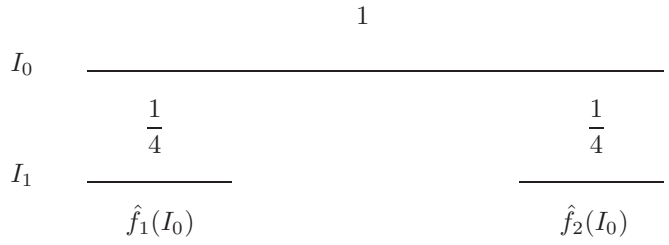

An application of the IFS parallel map on I_1 yields the following result,

$$\begin{aligned} \hat{\mathbf{f}}(I_1) &= \hat{f}_1(I_1) \bigcup \hat{f}_2(I_1) \\ &= \left[0, \frac{1}{16}\right] \bigcup \left[\frac{3}{16}, \frac{1}{4}\right] \bigcup \left[\frac{3}{4}, \frac{13}{16}\right] \bigcup \left[\frac{15}{16}, 1\right] \\ &= I_2 \,. \end{aligned} \tag{51}$$

Repeated action of this IFS produces a nested set of sets I_n which, in the limit $n \to \infty$, converges to a Cantor-like set – we'll call it $C_{1/4}$ – that lies in $[0, 1]$.

This limiting set is clearly not the **ternary Cantor set** – which would be called $C_{1/3}$ to be consistent – but it is a Cantor-like set. In fact, using the methods from the previous on fractal dimension, it should not be too difficult to see that the fractal dimension of this set is

$$D = \frac{\log\,(\text{no. of copies})}{\log\,(1/\text{scaling factor})} = \frac{\log 2}{\log 4} = \frac{1}{2} \,. \tag{52}$$

We may easily generalize this dissection procedure by considering the following two maps on $[0, 1]$,

$$f_1(x) = rx \,, \qquad f_2(x) = r(x-1) + 1 = rx + (1-r) \,, \tag{53}$$

where

$$0 < r < \frac{1}{2} \,. \tag{54}$$

Note that

$$f_1(0) = 0\,, \qquad f_2(1) = 1\,. \tag{55}$$

The action of the associated IFS parallel map $\hat{\mathbf{f}}$ on $I_0 = [0,1]$ is as follows,

$$\begin{aligned} \hat{\mathbf{f}}([0,1]) &= \hat{f}_1([0,1]) \bigcup \hat{f}_2([0,1]) \\ &= [0,r] \bigcup [1-r,1] \\ &= I_1\,. \end{aligned} \tag{56}$$

This IFS produces a dissection of [0,1] composed of two intervals of length r, as shown below.

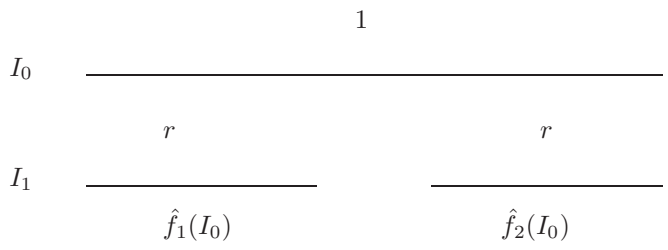

We saw this iteration procedure earlier in the course in connection with shifted Tent Maps on [0,1]. It produces a set of nested sets I_n which, in the limit $n \to \infty$, converge to a Cantor-like set C_r in [0,1]. Once again using the methods of the previous section on fractal dimension, the dimension of this Cantor set is found to be

$$D = \frac{\log\,(\text{no. of copies})}{\log \frac{1}{r}} = \frac{\log 2}{\log \frac{1}{r}}\,. \tag{57}$$

Special cases: Note that if we allow the parameter r to be $\frac{1}{2}$, then no dissection is performed, i.e.,

$$\begin{aligned} \hat{\mathbf{f}}([0,1]) &= \hat{f}_1([0,1]) \bigcup \hat{f}_2([0,1]) \\ &= \left[0, \frac{1}{2}\right] \bigcup \left[\frac{1}{2}, 1\right] \\ &= [0,1]\,. \end{aligned} \tag{58}$$

In other words, we have simply regenerated the interval $[0,1]$. As such, I_0 is a fixed point of the IFS. From Eq. (57), the (fractal) dimension of this set is

$$D = \frac{\log 2}{\log \frac{1}{1/2}} = 1\,, \tag{59}$$

which is consistent with the fact that the attractor is the interval $[0,1]$.

Let us now examine the case, $\frac{1}{2} < r < 1$. Here, the two sets

$$\hat{f}_1([0,1]) = [0,r]\,, \quad \hat{f}_2([0,1]) = [1-r,1]\,, \tag{60}$$

intersect. There is no dissection of the interval $[0,1]$. The union of these sets produces $[0,1]$. Unfortunately, the formula for the fractal dimension is not applicable here since the two sets overlap. The dimension for the attractor set $[0,1]$ is always 1.

The dissection procedure discussed above can be further generalized by allowing the contraction factors of the two maps to be independent, i.e.,

$$f_1(x) = rx\,, \qquad f_2(x) = s(x-1)+1 = sx + (1-s)\,, \tag{61}$$

where

$$0 < r < 1\,, \quad 0 < s < 1 \ \text{ and } r + s < 1\,. \tag{62}$$

Note that

$$f_1(0) = 0\,, \quad f_2(1) = 1\,. \tag{63}$$

The action of the associated IFS parallel map $\hat{\mathbf{f}}$ on $I_0 = [0,1]$ is as follows,

$$\begin{aligned} \hat{\mathbf{f}}([0,1]) &= \hat{f}_1([0,1]) \bigcup \hat{f}_2([0,1]) \\ &= [0,r] \bigcup [1-s,1] \\ &= I_1\,. \end{aligned} \tag{64}$$

This IFS produces a dissection of [0,1] composed of two intervals, one of length r and the other of length s as sketched below.

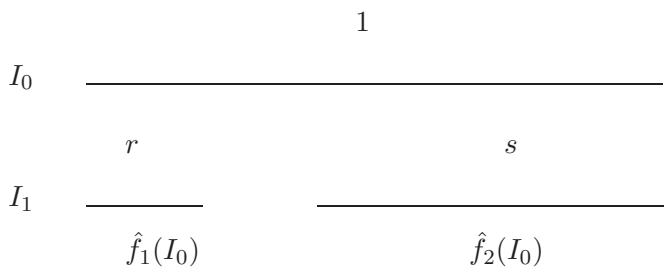

Repeated application of this IFS map will produce a nested set of intervals I_n which, in the limit $n \to \infty$, converges to a Cantor-like set $C_{rs} \subset [0,1]$. From our previous discussion of the fractal dimension, in particular, the generalized von Koch curves, the fractal dimension D_{rs} of the Cantor-like set C_{rs} will be the unique solution of the equation,

$$r^D + s^D = 1\,. \tag{65}$$

Unfortunately, no closed form expression for this solution exists, except in the special case that $0 < r = s < \frac{1}{2}$, in which case the above equation becomes

$$2r^D = 1 \quad \Longrightarrow \quad D = \frac{\log 2}{\log \frac{1}{r}}, \tag{66}$$

which is the result obtained earlier.

The von Koch curve

In a previous lecture, we showed that the von Koch curve, shown below,

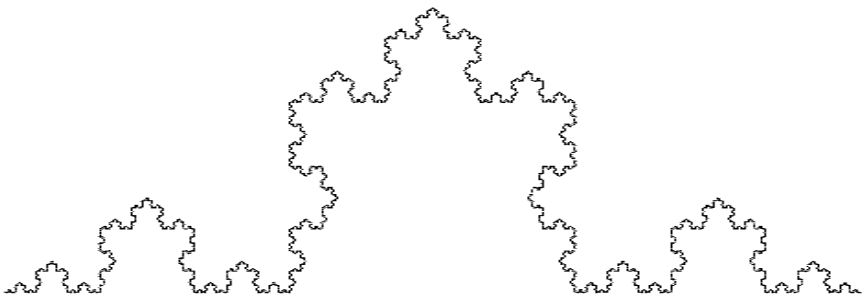

von Koch curve

may be produced by the repeated action of the following generator G,

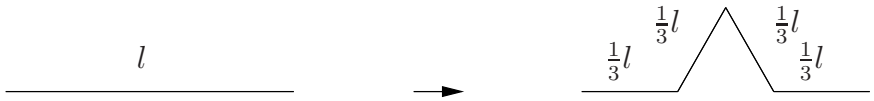

starting with the set $I_0 = [0, 1]$. We now show how this fractal curve can be generated by an IFS. We assume, once again, that the leftmost point of the curve is situated at (0,0) and rightmost point at (1,0).

Recall once again that the von Koch curve C is **self-similar**, i.e., it may be expressed as a union of four contracted copies of itself. Each contracted copy is one-fourth the size of C. This self-similarity could be seen to be built into the set from the generator G that was used to construct it.

The first copy, which starts at the point (0,0), is obtained by shrinking the von Koch curve by a factor

of $\frac{1}{3}$ toward (0,0) using the following affine map in $\mathbb{R}^2$:

$$f_1(x,y) = \begin{pmatrix} \frac{1}{3} & 0 \\ 0 & \frac{1}{3} \end{pmatrix} \begin{pmatrix} x \\ y \end{pmatrix} . \tag{67}$$

The second copy, which starts at the point $(\frac{1}{3},0)$ and ends at $(\frac{1}{2},\frac{\sqrt{3}}{6})$, may be obtained by first shrinking the von Koch curve toward (0,0) with contraction factor $\frac{1}{3}$, then rotating it by an angle $\frac{\pi}{3}$ and finally translating it in the x-direction by $\frac{1}{3}$.

Note: At this point, it might be helpful to recall the form of a rotation matrix in $\mathbb{R}^2$. The matrix $\mathbf{R}$ which rotates all points in the plane by an angle θ (counterclockwise for $\theta > 0$) with respect to the center point $(0,0)$ is as follows,

$$\mathbf{R} = \begin{pmatrix} \cos\theta & -\sin\theta \\ \sin\theta & \cos\theta \end{pmatrix} . \tag{68}$$

As a check, when $\theta = 0$, $\mathbf{R} = \mathbf{I}$, the identity matrix.

Returning to our main discussion, the following affine map will produce the second copy of the von Koch curve,

$$f_2(x,y) = \frac{1}{3} \begin{pmatrix} \frac{1}{2} & -\frac{\sqrt{3}}{2} \\ \frac{\sqrt{3}}{2} & \frac{1}{2} \end{pmatrix} \begin{pmatrix} x \\ y \end{pmatrix} + \begin{pmatrix} \frac{1}{3} \\ 0 \end{pmatrix} . \tag{69}$$

The third copy of the von Koch curve, which starts at the point $(\frac{1}{2},\frac{\sqrt{3}}{6})$, may be obtained by once again shrinking the von Koch curve toward (0,0) with contraction factor $\frac{1}{3}$, then rotating it by angle $-\frac{\pi}{3}$ and finally translating it to $(\frac{1}{2},\frac{\sqrt{3}}{6})$. all of these actions are accomplished with the following affine map,

$$f_3(x,y) = \frac{1}{3} \begin{pmatrix} \frac{1}{2} & \frac{\sqrt{3}}{2} \\ -\frac{\sqrt{3}}{2} & \frac{1}{2} \end{pmatrix} \begin{pmatrix} x \\ y \end{pmatrix} + \begin{pmatrix} \frac{1}{2} \\ \frac{\sqrt{3}}{6} \end{pmatrix} . \tag{70}$$

The fourth copy, which ends at (1,0), may be obtained by once again shrinking the von Koch curve toward (0,0) with contraction factor $\frac{1}{3}$ and then simply translating it to $(\frac{2}{3},0)$. This is accomplished with the following affine map,

$$f_4(x,y) = \begin{pmatrix} \frac{1}{3} & 0 \\ 0 & \frac{1}{3} \end{pmatrix} \begin{pmatrix} x \\ y \end{pmatrix} + \begin{pmatrix} \frac{2}{3} \\ 0 \end{pmatrix} . \tag{71}$$

We have achieved our goal: The four contraction maps f_i, $1 \le i \le 4$, produce four copies $\hat{f}_i(C)$ the von Koch curve C such that the union of these copies reproduces C, i.e.,

$$C = \bigcup_{i=1}^{4} \hat{f}_i(C) . \tag{72}$$

The results are summarized below.

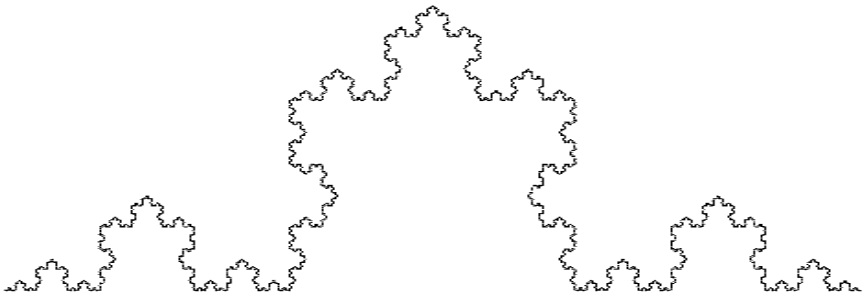

von Koch curve

$$f_1(x,y) = \begin{pmatrix} \frac{1}{3} & 0 \\ 0 & \frac{1}{3} \end{pmatrix} \begin{pmatrix} x \\ y \end{pmatrix} + \begin{pmatrix} 0 \\ 0 \end{pmatrix}$$

Contraction factor $r = \frac{1}{3}$, no rotation, no translation.

$$f_2(x,y) = \begin{pmatrix} \frac{1}{6} & -\frac{\sqrt{3}}{6} \\ \frac{\sqrt{3}}{6} & \frac{1}{6} \end{pmatrix} \begin{pmatrix} x \\ y \end{pmatrix} + \begin{pmatrix} \frac{1}{3} \\ 0 \end{pmatrix}$$

Contraction factor $r = \frac{1}{3}$, rotation $\pi/3$, translation.

$$f_3(x,y) = \begin{pmatrix} \frac{1}{6} & \frac{\sqrt{3}}{6} \\ -\frac{\sqrt{3}}{6} & \frac{1}{6} \end{pmatrix} \begin{pmatrix} x \\ y \end{pmatrix} + \begin{pmatrix} \frac{1}{2} \\ \frac{\sqrt{3}}{6} \end{pmatrix}$$

Contraction factor $r = \frac{1}{3}$, rotation $-\pi/3$, translation.

$$f_4(x,y) = \begin{pmatrix} \frac{1}{3} & 0 \\ 0 & \frac{1}{3} \end{pmatrix} \begin{pmatrix} x \\ y \end{pmatrix} + \begin{pmatrix} \frac{2}{3} \\ 0 \end{pmatrix}.$$

Contraction factor $r = \frac{1}{3}$, translation.

Sierpinski gasket

The Sierpinski gasket, seen before and shown below, is a union of three copies of itself, so we shall need three maps in the IFS. Each IFS map f_i will be a $\frac{1}{2}$ contraction with no rotation. The affine maps are quite easy to determine and are listed below.

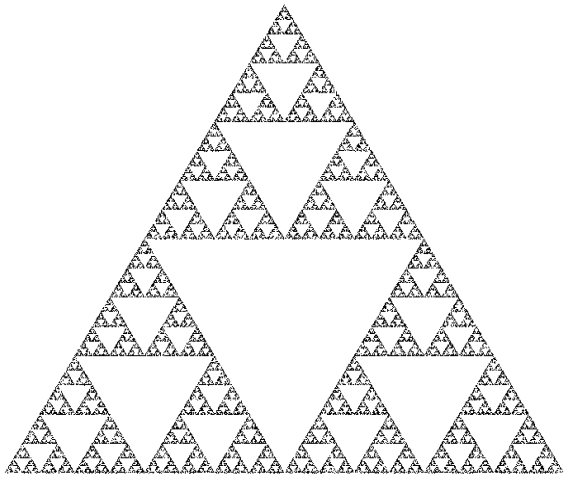

Sierpinski gasket

$$f_1(x,y) = \begin{pmatrix} \frac{1}{2} & 0 \\ 0 & \frac{1}{2} \end{pmatrix} \begin{pmatrix} x \\ y \end{pmatrix} + \begin{pmatrix} 0 \\ 0 \end{pmatrix}$$

Contraction factor $r = \frac{1}{2}$, rotation 0.

$$f_2(x,y) = \begin{pmatrix} \frac{1}{2} & 0 \\ 0 & \frac{1}{2} \end{pmatrix} \begin{pmatrix} x \\ y \end{pmatrix} + \begin{pmatrix} \frac{1}{4} \\ \frac{\sqrt{3}}{4} \end{pmatrix}$$

Contraction factor $r = \frac{1}{2}$, rotation 0, translation.

$$f_3(x,y) = \begin{pmatrix} \frac{1}{2} & 0 \\ 0 & \frac{1}{2} \end{pmatrix} \begin{pmatrix} x \\ y \end{pmatrix} + \begin{pmatrix} \frac{1}{2} \\ 0 \end{pmatrix}$$

Contraction factor $r = \frac{1}{2}$, rotation 0, translation.